Hindawi Publishing Corporation
Mathematical Problems in Engineering
Volume 2015, Article ID 242917, 9 pages
http://dx.doi.org/10.1155/2015/242917

Research Article

On the Vortex Detection Method Using Continuous Wavelet Transform with Application to Propeller Wake Analysis

Lifeng Wang,[1] Ruifeng Hu,[2] Jun Zhang,[3] and Yunpeng Ma[1]

[1]*School of Aeronautic Science and Technology, Beihang University, Beijing 100191, China*
[2]*School of Mechano-Electronic Engineering, Xidian University, Xi'an 710071, China*
[3]*China Ship Scientific Research Center, Wuxi 214082, China*

Correspondence should be addressed to Lifeng Wang; wanglf1972@163.com

Received 27 December 2014; Revised 12 May 2015; Accepted 19 May 2015

Academic Editor: Dane Quinn

The method based on the continuous wavelet transformation to detect and characterize two-dimensional vortex is analyzed for a synthetic flow and applied to vortex detection of propeller wake. The characteristics of a vortex, such as center location, core radius, and circulation, are extracted based on the Lamb-Oseen and Rankine vortex models, the latter of which is a novel attempt. The effects of various factors such as the difference scheme, the grid and scale discretization, transform variable, and vortex model on vortex detection have been investigated thoroughly. The method is further applied to identify the tip vortex in a propeller wake.

1. Introduction

Vortical structures exist widely in nature and engineering applications, either harmful or beneficial. Examples include vortex from wing-tip and fuselage of large airplane which may influence flight safety of the following successive aircraft, vortex shed from rotating rotor that could induce strong vibration of the structure and generate severe noise, and vortex rings generated by a jet which can enhance mixing and transportation process significantly.

Despite the universal existence in fluid dynamics, there is no widely accepted mathematic definition for vortex; instead several criteria [1–7] were developed to identify vortex from velocity fields which can be obtained from either PIV measurement or numerical simulation. For detection and quantitative characterization of vortex from two-dimensional velocity vector fields, for example, vortex center location, radius, and circulation, Vollmers [8] made a detailed review on common used methods, but some disadvantages exist to limit the usage of these techniques, such as manually selected threshold and the robustness to the numerical/experiment error. Therefore, an automatic and robust method for vortex detection and characterization is still needed.

Wavelet transform is a kind of signal analysis method and is extensively used in recent years. Compared to Fourier transform and short-time Fourier transform, wavelet transform has a larger range of applications, because the signals from the time domain and frequency domain can be analyzed simultaneously. Farge [9, 10] introduced the method of continuous wavelet transform (CWT) to fluid mechanics especially for turbulence research for the first time. Afterwards, the wavelet method has been widely used for detection of coherent structures in various turbulent flows [11–16]. Schram and colleagues [17–19] were the first to extract quantitative vortex characteristics using the CWT method. Varun et al. [20] improved the algorithm to capture the vortex shape accurately and achieve automatic batch processing of vortex. Cierpka et al. [21–23] applied the method to some aerodynamic separated flows. In addition, Perret [24] proposed a new CWT based vortex detection method by using the swirling strength as the transform variable.

In this paper, we give a new CWT based vortex detection method by using the Rankine vortex model in addition to the commonly used Lamb-Oseen model. We perform a comprehensive study of the detection method for a synthetic flow, to investigate the effects of difference scheme, grid and scale discretization, transform variable, and vortex model on

the detection results. This kind of analysis is still lacking in literature. Then the method is adopted to detect and characterize the tip vortex from the PIV data of a propeller wake. The conclusions of the paper are drawn in the final part.

2. The Vortex Detection Method

2.1. The Continuous Wavelet Transform. The wavelet transform is an effective technique to extract weak signal submerged in noise. The continuous wavelet transform (CWT) uses localized mother wavelet to expand the signal along space, scale, and direction [10]. In an n-dimensional space, the continuous wavelet transform of a function $f(\mathbf{x})$ is defined as

$$\langle \Psi_{l,\mathbf{x}',\theta} \mid f \rangle = \int_{\Omega} f(\mathbf{x})\, \Psi^{*}{}_{l,\mathbf{x}',\theta}(\mathbf{x})\, d\mathbf{x}, \tag{1}$$

in which $\Psi^{*}{}_{l,\mathbf{x}',\theta}(\mathbf{x})$ is the mother wavelet function, $\mathbf{x}$ the n-dimensional coordinate, l the scale factor, $\mathbf{x}'$ the translation parameter, θ the transform angle, and Ω the infinite n-dimensional space as the integral range.

The selection of the mother wavelet generally depends on the local distribution of target signal. For a two-dimensional vortex, the vorticity distribution around the vortex core is usually regarded as the Gaussian form. Therefore, the 2D Mexican hat function (Marr wavelet) is usually used as the mother wavelet for vortex detection

$$\Psi_l = \frac{1}{l}\left(2 - \frac{r^2}{l^2}\right)\exp\left(-\frac{r^2}{2l^2}\right), \tag{2}$$

where $r = \sqrt{(x-x')^2 + (y-y')^2}$.

In literature, there are several choices for the transform function $f(x, y)$, such as the vorticity field ω, the enstrophy (square of vorticity) ω^2, and the second invariant Q of the velocity gradient tensor. Their expressions in the two-dimensional Cartesian coordinate are

$$\begin{aligned}
\omega(x,y) &= \frac{\partial v}{\partial x} - \frac{\partial u}{\partial y},\\
\omega^2(x,y) &= \left(\frac{\partial v}{\partial x} - \frac{\partial u}{\partial y}\right)^2,\\
Q(x,y) &= \frac{\partial u}{\partial x}\frac{\partial v}{\partial y} - \frac{\partial v}{\partial x}\frac{\partial u}{\partial y},
\end{aligned} \tag{3}$$

$$\begin{aligned}
\omega(r,\theta) &= \frac{\partial V_\theta}{\partial r} + \frac{V_\theta}{r} - \frac{1}{r}\frac{\partial V_r}{\partial \theta},\\
\omega^2(r,\theta) &= \left(\frac{\partial V_\theta}{\partial r} + \frac{V_\theta}{r} - \frac{1}{r}\frac{\partial V_r}{\partial \theta}\right)^2,\\
Q(r,\theta) &= \frac{\partial V_r}{\partial r}\left(\frac{1}{r}\frac{\partial V_\theta}{\partial \theta} + \frac{V_r}{r}\right) - \frac{\partial V_\theta}{\partial r}\left(\frac{1}{r}\frac{\partial V_r}{\partial \theta} - \frac{V_\theta}{r}\right)
\end{aligned} \tag{4}$$

in the cylindrical coordinate.

The derivatives in (3) can be approximately evaluated by the standard 2nd-order central difference scheme, the 3rd-order Richardson scheme, or the velocity moment method. The wavelet transform is calculated using two-dimensional fast Fourier transform for the convolution in (1). The vortex is detected and the characteristics of the vortex are calculated through searching local maximum of the transformed results.

2.2. Vortex Detection Method Based on CWT and Lamb-Oseen Vortex Model. For the quantitative characterization of two-dimensional vortex, it is always assumed that the vortex obeys an analytical model, such as the Lamb-Oseen vortex model [25–27] which is most widely adopted, as

$$\begin{aligned}
V_\theta(r) &= \frac{\Gamma}{2\pi r}\left[1 - \exp\left(-\frac{r^2}{2\sigma^2}\right)\right],\\
\omega(r) &= \frac{\Gamma}{2\pi\sigma^2}\exp\left(-\frac{r^2}{2\sigma^2}\right),
\end{aligned} \tag{5}$$

where V_θ is the tangential velocity, r the distance from a point to the vortex center, σ a parameter related to vortex radius, and Γ the circulation of the vortex. At the edge of vortex, the tangential velocity V_θ approaches the local maximum, which leads to the vortex radius $\sigma_c = 1.585\sigma$. The circulation Γ of the Lamb-Oseen vortex satisfies

$$\Gamma = 2\pi\sigma^2\omega_m, \tag{6}$$

where ω_m is the maximum vorticity at the centroid of the vortex.

By substituting the vorticity of the Lamb-Oseen vortex model equation (5) and the Marr wavelet equation (2) into the wavelet transform equation (1), one can obtain

$$\begin{aligned}
\langle \Psi_l \mid \omega \rangle_{L-O} &= 2\pi \int_0^{\infty} \frac{\Gamma}{2\pi\sigma^2}\exp\left(-\frac{r^2}{\sigma^2}\right)\\
&\quad \cdot \frac{1}{l}\left(2 - \frac{r^2}{l^2}\right)\exp\left(-\frac{r^2}{2l^2}\right) r\, dr = \frac{2\Gamma l^3}{\left(l^2 + \sigma^2\right)^2}.
\end{aligned} \tag{7}$$

$\langle \Psi_l \mid \omega \rangle_{L-O}$ achieves its maximum when $l_m = \sqrt{3}\sigma$, and therefore the radius of the vortex satisfies $\sigma_c = 1.585\sigma = 0.915 l_m$.

By substituting the enstrophy of the Lamb-Oseen vortex model equation (5) and the Marr wavelet equation (2) into the wavelet transform equation (1), we can obtain

$$\begin{aligned}
\left\langle \Psi_l \mid \omega^2 \right\rangle_{L-O} &= 2\pi \int_0^{\infty} \frac{\Gamma^2}{4\pi^2\sigma^4}\exp\left(-\frac{r^2}{\sigma^2}\right)\\
&\quad \cdot \frac{1}{l}\left(2 - \frac{r^2}{l^2}\right)\exp\left(-\frac{r^2}{2l^2}\right) r\, dr = \frac{2\Gamma^2 l^3}{\pi\sigma^2\left(2l^2 + \sigma^2\right)^2}.
\end{aligned} \tag{8}$$

It also can be found that $\langle \Psi_l \mid \omega^2 \rangle_{L-O}$ achieves its maximum when $l_m = (\sqrt{6}/2)\sigma$. Then the radius of the vortex core is $\sigma_c = 1.585\sigma = 1.294 l_m$.

If the second invariant of velocity gradient tensor Q is used for wavelet transformation, we can get

$$\langle \Psi_l \mid Q \rangle_{L-O} = \frac{\Gamma^2}{\pi l^3 \sigma^2} \ln \frac{\left(l^2/\sigma^2 + 1\right)}{\sqrt{2l^2/\sigma^2 + 1}} - \frac{\Gamma^2}{4\pi l^3 \sigma^2} \left[1 - \frac{2}{l^2/\sigma^2 + 1} + \frac{1}{2l^2/\sigma^2 + 1}\right]. \tag{9}$$

And $\langle \Psi_l \mid Q \rangle_{L-O}$ achieves its maximum when $l_m = 1.095\sigma$. Thus the radius of vortex core is $\sigma_c = 1.585\sigma = 1.447 l_m$.

2.3. Vortex Detection Method Based on CWT and Rankine Vortex Model. The Rankine model [25–27] is another well-known two-dimensional analytical vortex solution, which combines a solid vortex core and an inviscid outer flow. The tangential velocity and vorticity distributions of the Rankine vortex are

$$V_\theta(r) = \begin{cases} \dfrac{\Gamma}{2\pi\sigma_c^2} r, & r \le \sigma_c, \\ \dfrac{\Gamma}{2\pi r}, & r > \sigma_c, \end{cases} \qquad \omega(r) = \begin{cases} \dfrac{\Gamma}{\pi\sigma_c^2}, & r \le \sigma_c, \\ 0, & r \le \sigma_c. \end{cases} \tag{10}$$

The circulation Γ of the Rankine vortex satisfies

$$\Gamma = \pi \sigma_c^2 \omega_m, \tag{11}$$

where ω_m is the vorticity in the core region of the vortex.

By substituting the vorticity, enstrophy, and the velocity gradient tensor's second invariant of the Rankine vortex model equations (10) and the Marr wavelet equation (2) into the wavelet transform equation (1), we obtain

$$\begin{aligned} \langle \Psi_l \mid \omega \rangle_R &= 2\pi \int_0^{\sigma_c} \frac{\Gamma}{\pi\sigma_c^2} \cdot \frac{1}{l} \left(2 - \frac{r^2}{l^2}\right) \exp\left(-\frac{r^2}{2l^2}\right) r\, dr \\ &= \frac{2\Gamma}{l} \exp\left(-\frac{\sigma_c^2}{2l^2}\right), \\ \left\langle \Psi_l \mid \omega^2 \right\rangle_R &= 2\pi \int_0^{\sigma_c} \frac{\Gamma^2}{\pi^2\sigma_c^4} \cdot \frac{1}{l} \left(2 - \frac{r^2}{l^2}\right) \exp\left(-\frac{r^2}{2l^2}\right) r\, dr \\ &= \frac{2\Gamma^2}{\pi\sigma_c^2 l} \exp\left(-\frac{\sigma_c^2}{2l^2}\right), \\ \langle \Psi_l \mid Q \rangle_R &= 2\pi \int_0^{\sigma_c} \frac{\Gamma^2}{4\pi^2\sigma_c^4} \cdot \frac{1}{l} \left(2 - \frac{r^2}{l^2}\right) \exp\left(-\frac{r^2}{2l^2}\right) r\, dr \\ &\quad - 2\pi \int_{\sigma_c}^{\infty} \frac{\Gamma^2}{4\pi^2 r^4} \cdot \frac{1}{l} \left(2 - \frac{r^2}{l^2}\right) \exp\left(-\frac{r^2}{2l^2}\right) r\, dr \\ &= \frac{\Gamma^2}{2\pi l} \left(\frac{1}{\sigma_c^2} - \frac{1}{2l^2}\right) \exp\left(-\frac{\sigma_c^2}{2l^2}\right). \end{aligned} \tag{12}$$

Table 1: Parameters for Lamb-Oseen vortices in synthetic flow.

Number	x_c	y_c	σ	σ_c	Γ
1	−0.50	0.50	0.05	0.08	1.0
2	0.50	0.50	0.075	0.12	2.25
3	0.0	0.0	0.05	0.08	2.0

Table 2: Comparison of vortex detection results for the synthetic flow with three difference schemes (relative error in bracket).

Number	Methods	x_c	y_c	σ_c	Γ
1	CDS	−0.48	0.48	0.101 (26%)	1.21 (21%)
	RDS	−0.48	0.48	0.091 (14%)	1.09 (9%)
	VMM	−0.52	0.52	0.101 (26%)	1.14 (14%)
2	CDS	0.48	0.48	0.130 (8%)	2.36 (5%)
	RDS	0.48	0.48	0.130 (8%)	2.50 (11%)
	VMM	0.52	0.52	0.130 (8%)	2.29 (2%)
3	CDS	0.0	0.0	0.081 (1%)	1.80 (10%)
	RDS	0.0	0.0	0.081 (1%)	2.00 (0%)
	VMM	0.0	0.0	0.091 (14%)	2.11 (6%)

$\langle \Psi_l \mid \omega \rangle_R$ and $\langle \Psi_l \mid \omega^2 \rangle_R$ reach their peaks when $l_m = \sigma_c$, while $\langle \Psi_l \mid Q \rangle_R$ achieves its maximum when $\sigma_c = 1.510 l_m$.

3. Vortex Detection for Synthetic Flow

In this section, we study the effectiveness of the wavelet based vortex detection and characterization method by applying it to a synthetic flow, which was introduced by Schram et al. [19] firstly. The synthetic flow extends from −1 to 1 in both x and y directions and is superimposed by three Lamb-Oseen vortices and a hyperbolic tangent shear layer. The values of these parameters for three Lamb-Oseen vortices are listed in Table 1. And the velocity distribution of the hyperbolic shear layer is

$$u_{\text{shear}}(x, y) = 3 \tanh\left[20\left(y + 5\right)\right]. \tag{13}$$

The velocity vector field and vorticity contour of the synthetic flow are displayed in Figure 1.

3.1. Effect of Difference Scheme. The effect of difference scheme for velocity derivative approximation on vortex detection result is investigated here, including the central difference scheme (CDS), the Richardson difference scheme (RDS), and the velocity moment method (VMM). Detection was carried out on a relatively coarse grid (51×51) using the Lamb-Oseen vortex model and enstrophy as the transform variable.

Table 2 shows the detection results using three difference schemes with relative errors. It is seen that the result using RDS is the best while VMM is the worst for vortex radius σ_c. For vortex circulation, the result using CDS is the worst, and RDS performs better for vortex number 1 and vortex number 3 than VMM except for vortex number 2. Overall, the detection accuracy would be degraded if the vortex is too weak, and RDS should be preferred to CDS and VMM.

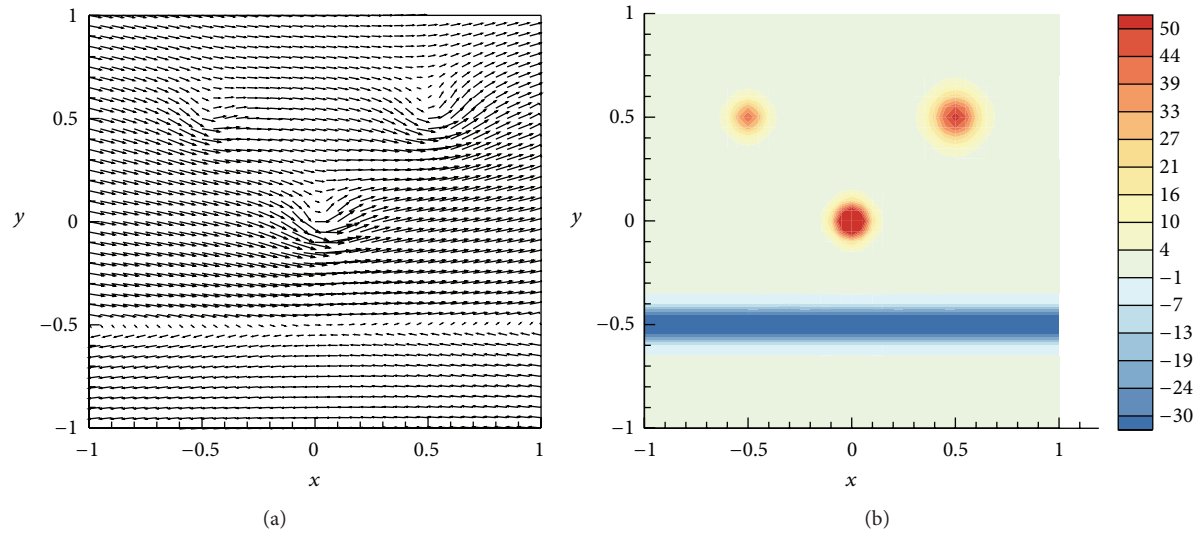

Figure 1: The synthetic flow: (a) velocity vectors, (b) vorticity contour.

Table 3: Comparison of vortex detection results for the synthetic flow with different grid sizes (relative error in bracket).

Number	Grid density	x_c	y_c	σ_c	Γ
1	51×51	−0.48	0.48	0.091 (14%)	1.09 (9%)
	101×101	−0.50	0.50	0.080 (0%)	1.01 (1%)
2	51×51	0.48	0.48	0.130 (8%)	2.50 (11%)
	101×101	0.50	0.50	0.119 (1%)	2.27 (1%)
3	51×51	0.0	0.0	0.081 (1%)	2.00 (0%)
	101×101	0.0	0.0	0.080 (0%)	2.03 (2%)

Table 4: Comparison of vortex detection results for the synthetic flow with different scale discretization intervals (relative error in bracket).

Number	Scale interval	x_c	y_c	σ_c	Γ
1	Δ	−0.50	0.50	0.078 (3%)	0.96 (4%)
	0.2Δ	−0.50	0.50	0.080 (0%)	1.01 (1%)
2	Δ	0.50	0.50	0.129 (8%)	2.66 (18%)
	0.2Δ	0.50	0.50	0.119 (1%)	2.27 (1%)
3	Δ	0.0	0.0	0.078 (3%)	1.91 (5%)
	0.2Δ	0.0	0.0	0.080 (0%)	2.03 (2%)

3.2. Effects of Grid and Scale Discretization. The sensitivity of vortex detection result on the grid size is studied in this section. We select one coarse grid (51×51) and one fine grid (101×101) for comparison. Detection was carried out using the Lamb-Oseen vortex model and enstrophy as the transform variable, and the derivatives were approximated by RDS. Table 3 shows the detection results using two grids with relative errors. The relative errors for vortex radius and circulation detection results are all less than 3% on the fine grid, which is a much great improvement compared to those on the coarse grid. In other words, there should be at least around 10 grid points in the vortex core to characterize vortical structure in a high accuracy.

The discretization of the scale l is another important parameter which could affect the detection accuracy. Here we choose two scale discretization intervals for comparison, that is, $\delta l = \Delta$ and $\delta l = 0.2\Delta$, where Δ is the discretized grid size. Detection was carried out using the Lamb-Oseen vortex model and enstrophy as the transform variable, and the derivatives were approximated by RDS on a 101×101 grid. The detection results and relative errors are listed in Table 4. It is shown that the detection accuracy can be improved by reducing the discretization interval of the scale l, and the detection result of the vortex with large radius (vortex number 2) is more sensitive to the value of δl.

3.3. Effects of Transform Variable and Vortex Model. In this part, we analyze the performance of transform variable, that is, the vorticity, enstrophy, and the second invariant of velocity gradient tensor, on vortex detection. Detection was carried out using the Lamb-Oseen vortex model and the derivatives were approximated by RDS on a 101×101 grid. In Table 5, it is seen that the detection result based on enstrophy is a little better than the other two in general.

Furthermore, we compare the detection results using Lamb-Oseen and Rankine vortex models. Detection was carried out using the enstrophy as transform variable and the derivatives were approximated by RDS on a 101×101 grid. Table 6 shows the detection results, and the use of Rankine vortex model leads to a relative deviation of detection around 25%. It is not surprising since the synthetic flow is made of Lamb-Oseen vortex.

Table 5: Comparison of vortex detection results for the synthetic flow with different transform variables (relative error in bracket).

Number	Transform variables	x_c	y_c	σ_c	Γ
1	ω	−0.50	0.50	0.081 (1%)	1.03 (3%)
	ω^2	−0.50	0.50	0.080 (0%)	1.01 (1%)
	Q	−0.50	0.50	0.081 (1%)	1.04 (4%)
2	ω	0.50	0.50	0.117 (3%)	2.18 (3%)
	ω^2	0.50	0.50	0.119 (1%)	2.27 (1%)
	Q	0.50	0.50	0.122 (2%)	2.35 (4%)
3	ω	0.0	0.0	0.081 (1%)	2.06 (3%)
	ω^2	0.0	0.0	0.080 (0%)	2.03 (2%)
	Q	0.0	0.0	0.081 (1%)	2.08 (4%)

Table 6: Comparison of vortex detection results for the synthetic flow with different vortex models (relative error in bracket).

Number	Vortex model	x_c	y_c	σ_c	Γ
1	Lamb-Oseen	−0.50	0.50	0.080 (0%)	1.01 (1%)
	Rankine	−0.50	0.50	0.060 (25%)	0.72 (28%)
2	Lamb-Oseen	0.50	0.50	0.119 (1%)	2.27 (1%)
	Rankine	0.50	0.50	0.092 (23%)	1.69 (25%)
3	Lamb-Oseen	0.0	0.0	0.080 (0%)	2.03 (2%)
	Rankine	0.0	0.0	0.060 (25%)	1.43 (29%)

4. Vortex Detection for Propeller Wake

In this section, the CWT based vortex detection method was used to identify and characterize vortex from a propeller tip. The propeller wake analysis is an active topic in hydrodynamics and marine engineering; see [28–33], for instance. However, few attempts have been carried out to extract vortex features quantitatively in propeller wake.

The experiment was conducted in the cavitation water channel of China Ship Scientific Research Center. The cavitation water channel has a test section with 3200 mm in length and 800 mm in diameter. The water speed is 3~20 m/s. Standard propeller DTMB-P4119 with diameter of 250 mm was used in the present study. It is a right-handed three-blade propeller with the hub/diameter ratio of 0.2 and radius R of 0.1 m without pitching. In the experiment, the freestream speed U is 4.32 m/s, the propeller revolution frequency is 20 Hz, and the advance coefficient is 0.863.

The propeller and PIV system is schematically shown in Figure 2. Two Surelite II-10Na-YAG solid pulsed lasers were used as the light source which illuminated the flow field from side window of the water tunnel. One Megaplus 2.0 CCD camera (2048 pixels × 2048 pixels) with a Nikon 50f1.4 lens was used to record the particle image. Pollen pini which is 40 μm in diameter was adopted as tracer particles. Phase-averaged velocity field was obtained by averaging of 50 sets of velocity data in the same rotation phase. Phase-averaged vorticity distribution at a specific instant is shown in Figure 3, in which the tip vortex shed from the propeller

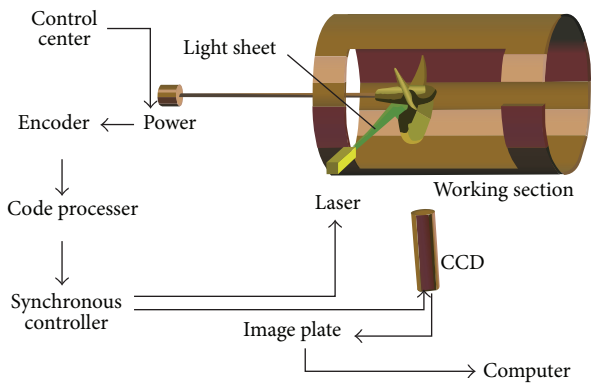

Figure 2: Schematic illustration of propeller and PIV system.

can be identified. The derivatives of velocity were calculated approximately using the Richardson difference scheme.

The detected trajectory of propeller wake vortex is displayed in Figure 4, from which an obvious radial contraction phenomenon is observed. The radial contraction of propeller wake in near-wake region has been reported by many studies [28–32]. We compared the effect of different transform variables on detection results. As in Figure 5 for evolution of the propeller vortex radius and circulation along its trajectory, it is found that the detection results are more scattered by using ω^2 and Q than ω as the transform variable. Outputs by the Lamb-Oseen and Rankine vortex models were compared in Figure 6, and there are some quantitative differences between them but the detection results are similar qualitatively. We also compared the tangential velocity distributions between experimental measurement and reconstructions from detection result and vortex models, as shown in Figure 7. The vortex model parameters were determined from detection results using vorticity ω as the transform variable. It is observed that the Lamb-Oseen vortex model behaves better than the Rankine model near the edge of vortex, while they both underpredict the tangential velocity in the region away from vortex core.

5. Conclusions

The continuous wavelet based vortex detection method is analyzed and applied to propeller wake analysis in this paper. And a method based on the Rankine vortex model is given, which is a new attempt. The final conclusions are drawn in the following:

(1) According to the detection results for a synthetic flow, it is suggested that the Richardson difference scheme is preferred to the central difference scheme and the velocity moment method for derivatives approximation. For the requirement of grid discretization, there should be at least 10 grid points in the vortex core region to achieve high accuracy. The detection can be improved by reducing the discretization interval of the scale parameter.

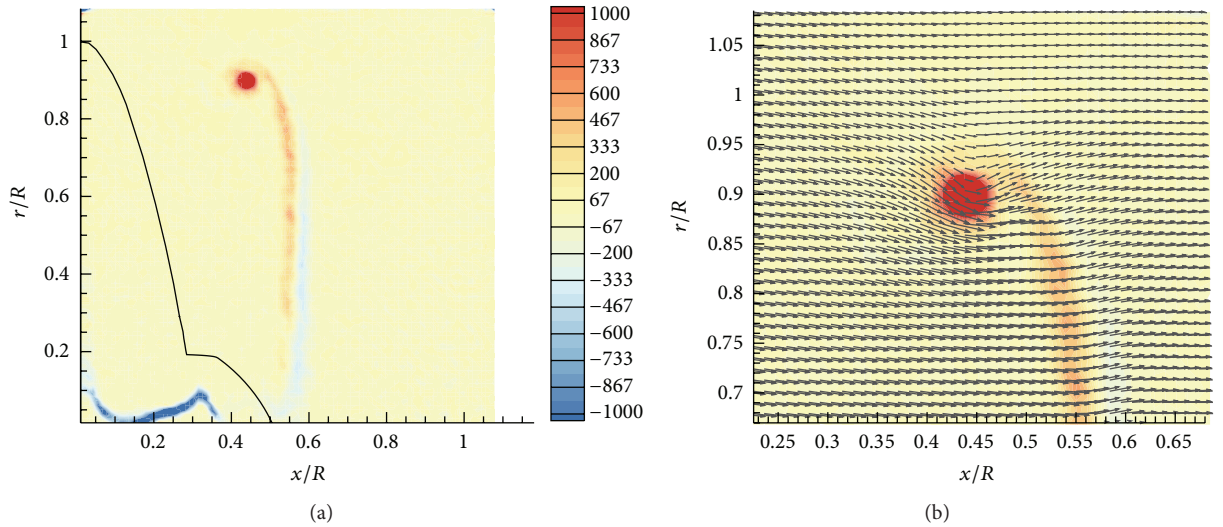

Figure 3: Propeller flow field: (a) vorticity contour, (b) zoomed-in vorticity field superposed with velocity vectors.

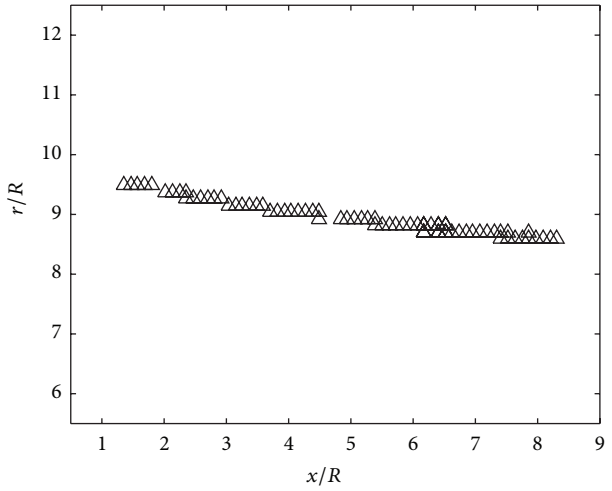

Figure 4: Trajectory of the propeller vortex.

(2) Also based on the results for the synthetic flow, the detection result using enstrophy as transform variable is a little better than using vorticity and the second variant of velocity gradient tensor. The use of the Rankine vortex model would lead to a relative detection error of 25% or so for a Lamb-Oseen vortex.

(3) By applying the CWT based vortex detection method to a propeller flow measured from PIV, it is found that the propeller tip vortex center presents a radial contraction pattern, and the detection results for vortex radius and circulation are more scattered by using enstrophy ω^2 and Q than vorticity ω. The reason for the scattering is not clear and we speculate it to be environmental noise and insufficient spatial resolution of PIV measurement. Therefore, how to improve the performance of the CWT based vortex detection method for a flow field with significant noise and insufficient spatial resolution should be studied in future.

Conflict of Interests

The authors declare that there is no conflict of interests regarding the publication of this paper.

Authors' Contribution

Lifeng Wang and Ruifeng Hu contributed equally to this work.

Acknowledgments

This work was supported by the National Natural Science Foundation of China (no. 51307004) and the Fundamental Research Funds for the Central Universities of China (no.

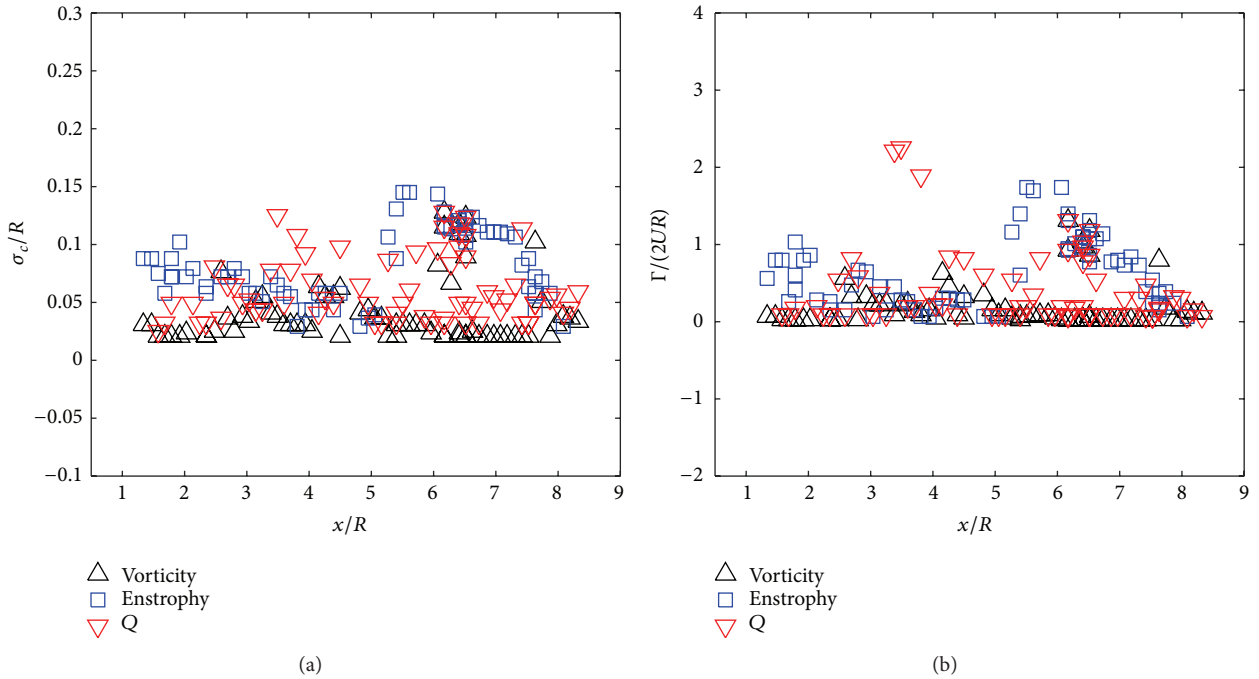

FIGURE 5: Evolution of the propeller vortex characteristics along its trajectory detected by CWT with Lamb-Oseen vortex model and different transform variables: (a) vortex radius; (b) vortex circulation.

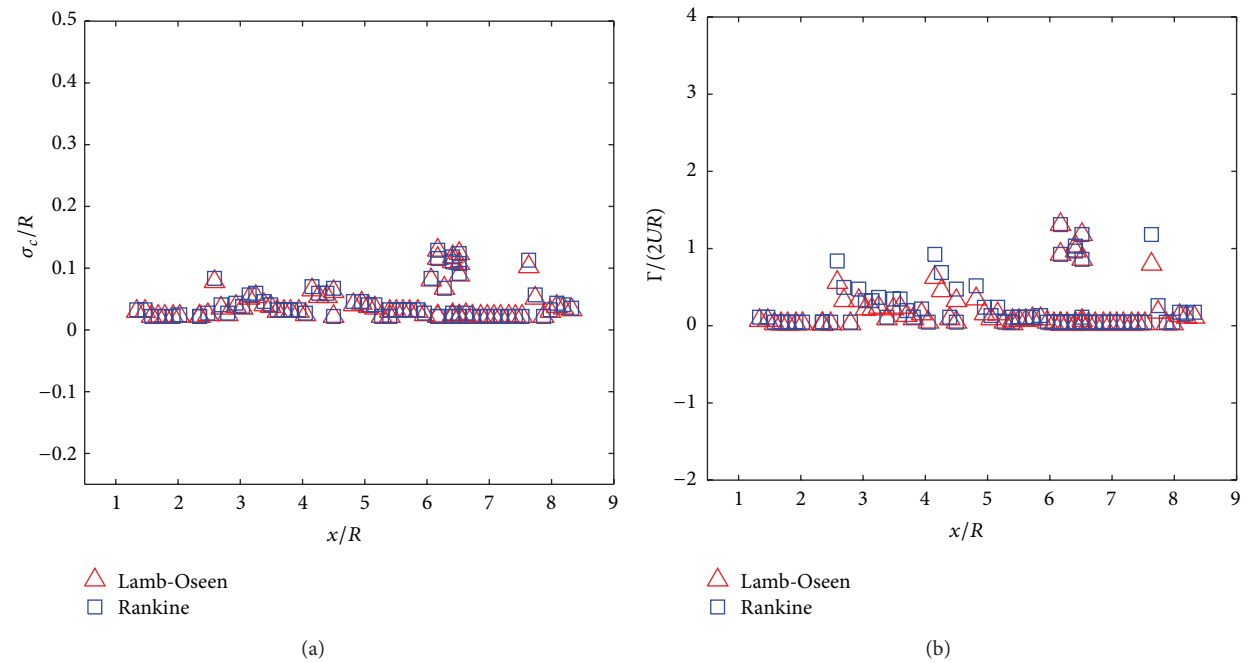

FIGURE 6: Evolution of the propeller vortex characteristics along its trajectory detected by CWT with different vortex models (Q for the transform variable): (a) vortex radius; (b) vortex circulation.

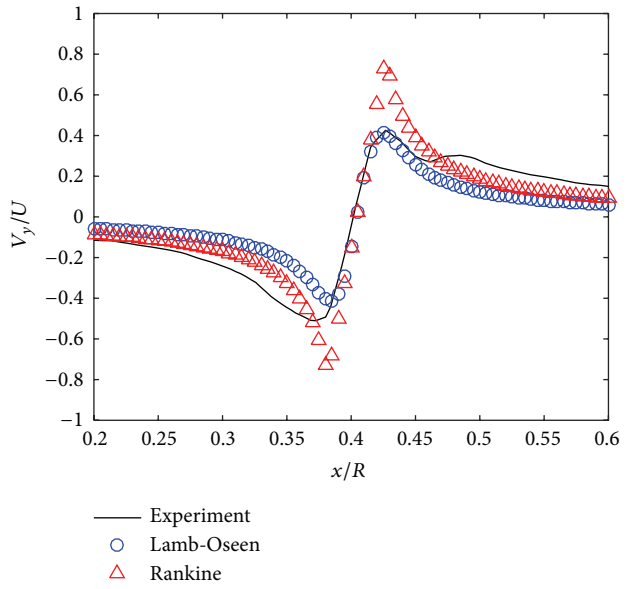

FIGURE 7: Comparison of tangential velocity distributions measured from experiment and reconstructed by the Lamb-Oseen and Rankine vortex models.

JB140418). The authors are grateful for helpful discussion with Dr. Christian Cierpka on the wavelet transform.

References

[1] J. C. R. Hunt, A. A. Wray, and P. Moin, "Eddies, stream, and convergence zones in turbulent flows," Report, Center for Turbulence Research, 1988.

[2] M. S. Chong, A. E. Perry, and B. J. Cantwell, "A general classification of three-dimensional flow fields," *Physics of Fluids A*, vol. 2, no. 5, pp. 765–777, 1990.

[3] J. Jeong and F. Hussain, "On the identification of a vortex," *Journal of Fluid Mechanics*, vol. 285, pp. 69–94, 1995.

[4] G. Haller, "An objective definition of a vortex," *Journal of Fluid Mechanics*, vol. 525, pp. 1–26, 2005.

[5] P. Chakraborty, S. Balachandar, and R. J. Adrian, "On the relationships between local vortex identification schemes," *Journal of Fluid Mechanics*, vol. 535, pp. 189–214, 2005.

[6] J.-Z. Wu, A.-K. Xiong, and Y.-T. Yang, "Axial stretching and vortex definition," *Physics of Fluids*, vol. 17, no. 3, Article ID 038108, 2005.

[7] K. Nakayama, K. Sugiyama, and S. Takagi, "A unified definition of a vortex derived from vortical flow and the resulting pressure minimum," *Fluid Dynamics Research*, vol. 46, no. 5, pp. 55511–55521, 2014.

[8] H. Vollmers, "Detection of vortices and quantitative evaluation of their main parameters from experimental velocity data," *Measurement Science and Technology*, vol. 12, no. 8, pp. 1199–1207, 2001.

[9] M. Farge, Y. Guezennec, C. M. Ho, and C. Meneveau, "Continuous wavelet analysis of coherent structures," Center for Turbulence Research Report, 1990.

[10] M. Farge, "Wavelet transforms and their applications to turbulence," *Annual Review of Fluid Mechanics*, vol. 24, pp. 395–457, 1992.

[11] S. V. Kailas and R. Narasimha, "The eduction of structures from flow imagery using wavelets part I. The mixing layer," *Experiments in Fluids*, vol. 27, no. 2, pp. 167–174, 1999.

[12] R. J. Adrian, K. T. Christensen, and Z.-C. Liu, "Analysis and interpretation of instantaneous turbulent velocity fields," *Experiments in Fluids*, vol. 29, no. 3, pp. 275–290, 2000.

[13] R. Camussi, "Coherent structure identification from wavelet analysis of particle image velocimetry data," *Experiments in Fluids*, vol. 32, no. 1, pp. 76–86, 2002.

[14] R. Camussi and F. Di Felice, "Statistical properties of vortical structures with spanwise vorticity in zero pressure gradient turbulent boundary layers," *Physics of Fluids*, vol. 18, no. 3, Article ID 035108, 16 pages, 2006.

[15] H.-B. Hu, P. Du, S.-H. Huang, and Y. Wang, "Extraction and verification of coherent structures in near-wall turbulence," *Chinese Physics B*, vol. 22, no. 7, Article ID 074703, 2013.

[16] K. V. Bulusu, S. Hussain, and M. W. Plesniak, "Determination of secondary flow morphologies by wavelet analysis in a curved artery model with physiological inflow," *Experiments in Fluids*, vol. 55, no. 11, 2014.

[17] C. Schram and M. L. Riethmuller, "Vortex ring evolution in an impulsively started jet using digital particle image velocimetry and continous wavelet analysis," *Measurement Science and Technology*, vol. 12, no. 9, pp. 1413–1421, 2001.

[18] C. Schram and M. L. Riethmuller, "Measurement of vortex ring characteristics during pairing in a forced subsonic air jet," *Experiments in Fluids*, vol. 33, no. 6, pp. 879–888, 2002.

[19] C. Schram, P. Rambaud, and M. L. Riethmuller, "Wavelet based eddy structure eduction from a backward facing step flow investigated using particle image velocimetry," *Experiments in Fluids*, vol. 36, no. 2, pp. 233–245, 2004.

[20] A. V. Varun, K. Balasubramanian, and R. I. Sujith, "An automated vortex detection scheme using the wavelet transform of the d_2 field," *Experiments in Fluids*, vol. 45, no. 5, pp. 857–868, 2008.

[21] C. Cierpka, T. Weier, and G. Gerbeth, "Evolution of vortex structures in an electromagnetically excited separated flow," *Experiments in Fluids*, vol. 45, no. 5, pp. 943–953, 2008.

[22] C. Cierpka, T. Weier, and G. Gerbeth, "Synchronized force and particle image velocimetry measurements on a NACA 0015 in poststall under control of time periodic electromagnetic forcing," *Physics of Fluids*, vol. 22, no. 7, Article ID 075109, 2010.

[23] Y.-H. Kim, C. Cierpka, and S. T. Wereley, "Flow field around a vibrating cantilever: coherent structure eduction by continuous wavelet transform and proper orthogonal decomposition," *Journal of Fluid Mechanics*, vol. 669, pp. 584–606, 2011.

[24] L. Perret, "PIV investigation of the shear layer vortices in the near wake of a circular cylinder," *Experiments in Fluids*, vol. 47, no. 4-5, pp. 789–800, 2009.

[25] G. L. Lamb, *Hydrodynamics*, Cambridge University Press, Cambridge, UK, 1932.

[26] P. G. Saffman, *Vortex Dynamics*, Cambridge University Press, Cambridge, UK, 1992.

[27] J. Z. Wu, H. Y. Ma, and M. D. Zhou, *Vorticity and Vortex Dynamics*, Springer, Berlin, Germany, 2006.

[28] B. G. Paik, C. M. Lee, and S. J. Lee, "PIV analysis of flow around a container ship model with a rotating propeller," *Experiments in Fluids*, vol. 36, no. 6, pp. 833–846, 2004.

[29] S. J. Lee, B. G. Paik, J. H. Yoon, and C. M. Lee, "Three-component velocity field measurements of propeller wake using a stereoscopic PIV technique," *Experiments in Fluids*, vol. 36, no. 4, pp. 575–585, 2004.

[30] B.-G. Paik, J. Kim, Y.-H. Park, K.-S. Kim, and K.-K. Yu, "Analysis of wake behind a rotating propeller using PIV technique in a cavitation tunnel," *Ocean Engineering*, vol. 34, no. 3-4, pp. 594–604, 2007.

[31] M. Felli and M. Falchi, "Propeller tip and hub vortex dynamics in the interaction with a rudder," *Experiments in Fluids*, vol. 51, no. 5, pp. 1385–1402, 2011.

[32] M. Felli, R. Camussi, and F. Di Felice, "Mechanisms of evolution of the propeller wake in the transition and far fields," *Journal of Fluid Mechanics*, vol. 682, pp. 5–53, 2011.

[33] A. Segalini and P. H. Alfredsson, "A simplified vortex model of propeller and wind-turbine wakes," *Journal of Fluid Mechanics*, vol. 725, pp. 91–116, 2013.